SIMULATION OF TURBULENT FLOW IN A TWO-STROKE GRAIL ENGINE CYLINDER

Shoeb Ahmed Syed[1]*, Peter O. Oyekola[2]

[1] Department of Mechanical Engineering, Papua New Guinea University of Technology, PNG
[2] Department of Mechanical Engineering, Tennessee Tech University, Cookeville, USA

* shoeb.syed@pnguot.ac.pg

This paper investigates the implementation of computational fluid dynamics for the analysis of a grail internal combustion engine. This is intended to analyse the intake hole and channel shape variables as well as their corresponding influence on the fluid flow properties within the cylinder. Due to the geometry of the engine design which features an intake valve positioned directly on the piston, the combustion efficiency is therefore heavily dependent on the flow characteristics. This necessitates the need to understand and analyse the effects of intake hole and duct geometry as well as piston motion on flow dynamics. A numerical simulation using Autodesk CFD finite element solver was used to simulate the engine flow dynamics of the Grail engine. The results of the analysis show a violent tornado-like effect in the flow field as well as an observable swirl effect characterized by a cylinder-centred single vortex. The resultant flow field obtainable from the design of the Grain engines will therefore allow an ideal homogeneous/stoichiometric fuel-air mixture for increased combustion efficiency. The result of both 3-D static and dynamic simulations of the flow through the engine provided guidelines on the selection of several geometrical parameters for optimal performance. The pressure inside the cylinder of the Grail Engine is validated with the experimental setup. The values of TKE obtained from the numerical simulation are well within the limits obtained from the references.

Keywords: grail engine, two-stroke engine, autodesk CFD simulation

1 INTRODUCTION

Internal combustion (IC) engines are a significant power production machine currently given their reliability, mobility, power-to-weight ratio, and general cost as compared to other counterparts. The general engine classification in the market is the two and four-stroke engines. The advantages of the two-stroke engines are design simplicity, reduced cost of maintenance as well as enhanced power output. However, this advantage comes at the cost of pollution due to the generation of smoke, and constant lubrication requirement using fuel oil mixture which further contributes to pollution-related issues. Due to this downside, the two-stroke engines have struggled to meet up with the requirements for implementation in the automobile industry however, they are commonly found in markets requiring small engines such as in boats, domestic food processing machines, motorcycles, etc.

Grail engine was designed as a two-stroke engine specifically to address the associated limitations of the standard two-stroke engines in the market. In this regard, the engines eliminate the need for the mixture of fuel and oil for lubrication by implementing a lubrication system modelled after the standard four-stroke IC engines [1].

The Grail engine [2] utilizes separate tubes/channels which inject compressed air into the cylinder as well as an inlet valve embedded in the piston center while the exhaust valve is strategically located at the top of the cylinder to achieve thorough scavenging and elimination of cross-contamination of oil (and fuel and air as prevailing IC engines) as there are no side ports also, there are three spark plugs positioned around the exhaust valve and a fuel injector on the cylinder head as in figure 1. This new design concept offers a solution that can potentially revolutionize the present market as it is designed to be capable of operating using a variety of fuels, increasing efficiency as well as reducing emissions [1].

This unique design [2] introduced the "Grail cycle" concept which is a combination of the homogeneous-charged compression ignition which simultaneously operates with the "Miller cycle" and forced semi-homogeneous-charged compression ignition (FS-HCCI). In the cylinder of IC engines, the fluid flow is characterized by extreme velocities associated with a large Reynolds number that indicated the occurrence of turbulent flow. This governs the propagation of flames during the spark-ignition as well as affects the mixing rate of air-fuel in the cylinder [3]. This fluctuating flow that affects the mixtures also affects the transfer of energy, mass and species concentrations more efficiently as compared with the absence of turbulence. Furthermore, the turbulence flow experienced also determines the nature of combustion within the cylinder such that the exhaust emission can be controlled. Therefore, an understanding of the flow pattern is necessary to optimize engine performance.

Journal of Applied Engineering Science

Vol. 20, No. 4, 2022
www.engineeringscience.rs

iipp
publishing

Shoeb Ahmed Syed et al. - Simulation of turbulent flow in a two-stroke grail engine cylinder
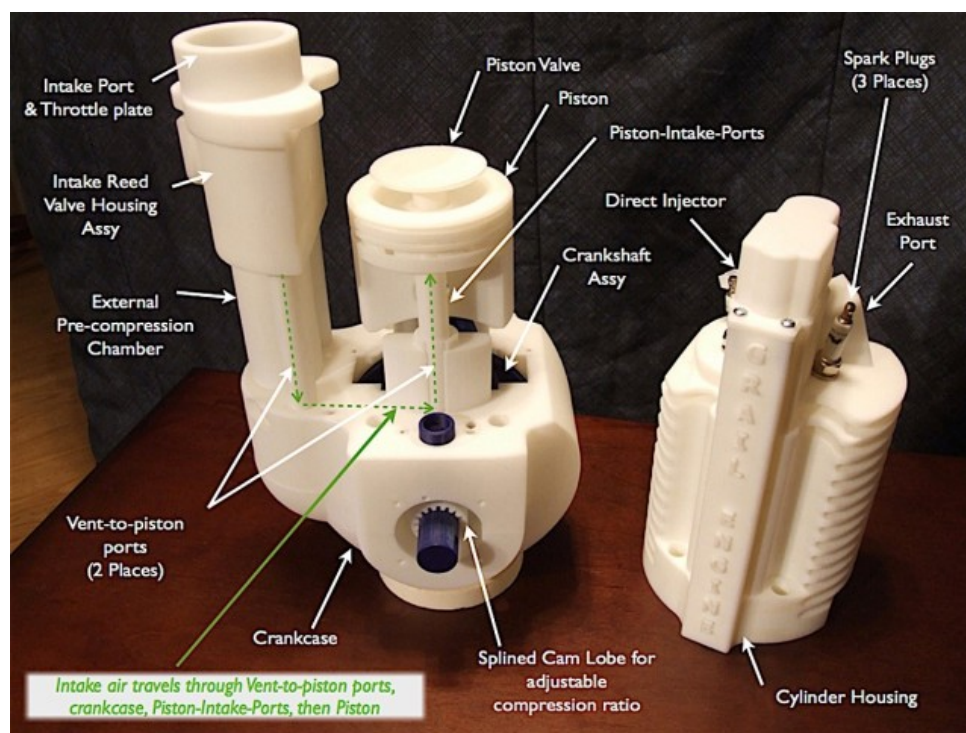
Fig. 1. design and Specifications of the Grail engine [2]

Generally, the particle image velocimetry (PIV) and laser Doppler velocimetry (LDV) methods have been applied in measuring the flow within the cylinder of IC engines depending on the focus of the research. The PIV method was applied in evaluating the cylinder flow of a premixed charge compression ignition (PCCI) engine through instantaneous velocity measurements as well as the measurement of turbulence intensities [4]. In the same vein, PIV was applied in the investigation of the tumble flow of a flat piston engine at varying speeds during its intake and compression stroke. according to the result of their study, the flow tumble ratio was dependent on the crank angle position and the increased operational speed of the engine correspondingly increased the maximum turbulent kinetic energy (TKE) towards the compression strokes end [5].

Similarly, for a single-cylinder engine, Li et al. [6] implemented a digital PIV methodology in estimating the fluctuations of velocity, turbulent length scale, vorticity as well as the strain rate which their results show that the spatial variation of the TKE distribution, as well as the velocity within the cylinder, was due to the low-frequency fluctuations of velocity component. In a separate study on a SI engine, the production of cylinder tumbling flow from the valves was measured using PIV where it was observed that upon commencement of the intake stroke to the end of the compression stroke, there was symmetrical flow distribution perpendicular to the cylinder axis [7]. Other applications of the PIV technique are seen in high-image-density PIV used in measuring velocity distribution [8], as well as in studying barrel swirl ratio (BSR) of engines [9].

LDV, on the other hand has been also employed in velocity measurements of engines [10], [11]where LDV was used to measure the boundary layers to mimic the heat transfer geometry probe. As well as in the study of the piston bowl effect on structure created during the intake stroke Payri et al. [12]. Heywood [13] investigated an IC engine and showed that the high turbulence experienced at the end of the compression stroke was a result of the generation of tumble and swirl vortices during the intake stroke which eventually led to better engine combustion efficiency.

Using particle tracking velocimetry (PTV), Kuwahara and Ando [14] studied the cylinder flow within the combustion chamber of a premixed lean burn and a GDI engine. They showed that better turbulence generation enhances controlled combustion. This was further validated in the result of Verbeek et al [15] which stated that the flow pattern (swirl and tumble) must be at an optimum level for efficient turbulence during the combustion process.

Due to the limitations of the standard experimental techniques as well as the relative cost associated with the analysis of flow parameters as well as other engine analysis, the Computational fluid dynamics (CFD) simulation has become an industry-standard frequently used in engine analysis. In this case, the optimization of key design parameters such as the valves geometry, location of injectors, sparkplugs, etc. can be simulated with various CFD codes such as KIVA [16], STAR-CD [17], FIRE [18], [19], ANSYS Fluent [20] and CFX [21]. Therefore, this study aims to simulate the dynamics of cylinder flow as well as in modelling the turbulence efficiency of the grail engine through a combination of static and dynamics mesh simulation of the intake valves and channel. This is done in other to optimize the profile geometry in other to support the adequate generation of turbulent kinetic energy as well as in performance improvement.

1.1 Engine working principle

Fluid flow regime through the grail engine cylinder varies its characteristics based on the stage of the flow. In the initiation of the intake stroke, the piston travels upward which creates a vacuum within the tube channels which allows the flow of fresh air charge through the one-way reed valves in form of a jet which is defined by the parameters of the port, timing, and valves. This creates large-scale turbulent flow motion comprising swirl and tumble [13] which accelerates the transport of the air-fuel mix throughout the cylinder uniformly the parameters of engine design (i.e., exhaust valves, ports, etc.) induce swirl or tumble motion. This turbulent motion reduces significantly at the proceeding stage of the intake stroke due to the fluid viscosity causing loss of energy.

Subsequently, as compression occurs the fuel is directly injected, and the mixture is compressed which causes density increase and change in the turbulent length scale. At this point, the swirl vorticity amount remains unchanged. However, there is a break in the tumble vortices contributing to increased turbulence level at ignition [22]. This results in magnified turbulence with corresponding viscous decay and continued transport which enhances the combustion stroke of the engine at TDC with three sparks ignition. Finally, in the exhaust stage piston moves downwards thereby creating compressive pressure in the tube channels. This allows fresh air intake simultaneously with the release of burnt gases from the exhaust valve. There is minimal turbulence at the exhaust stroke and the cycle repeats.

2 METHODOLOGY

Solving the turbulent flow of practical problems involves significant computational effort which can be applied to solve the governing equations. In this paper, the Autodesk CFD finite element solver was applied in solving the three governing equations while applying the finite element Galerkin's weighted residuals discretization method. The implicit segregated solver, as well as the monotone, streamline upwind scheme was applied to solve the compressible flow equations while the governing systems of equations for the flow within the cylinder were the compressible Navier-Stokes's equations with the PDEs are shown below [23] [24]:

Continuity equation:
$$\nabla.(\rho V) = 0 \qquad (1)$$

Momentum equation:
$$\rho(V.\nabla V) = \rho g - \nabla P + (\mu + \mu_t)\nabla^2 V + S_\omega + S_{DR} \qquad (2)$$

Energy equation:
$$C_p(V.\nabla T) = (k + k_t)\nabla^2 T + q_V \qquad (3)$$

The CFD codes used, allow for multi-block grid possibility which comes in handy for efficient execution in clustered parallel mode. The segregated implicit unsteady double precision solver was applied in the time-averaged numerical simulation. The turbulence model was based on the RANS standardized K-ε turbulence model [25] where the default values of the model were applied given its generic and numerous applications while using a second-order implicit scheme. This presented a more practical alternative to the LES model (which can be used to predict high Reynolds number flow) due to its lower computational requirement.

With the pressure-sensitive prediction of turbulence within the cylinder, the numerical diffusion is reduced, and a higher-order scheme is adopted for computation where the segregated solver utilized a SIMPLE-R algorithm. The boundary conditions used in the simulation study were based on an inlet and outlet pressure of 10 psig and 0 psig respectively where the pressure difference drives the flow. Similarly, the flow across the boundary was assumed to be fully turbulent and the air was modelled to be an ideal gas. Also, fluid and solid regions were constrained using wall boundary conditions with no-slip conditions pre-set at the walls. The flow also was assigned a no-slip condition with no pressure gradient and an adiabatic thermal condition governing the viscous solid surfaces.

The simulation study adopted the ADVI scheme where the convection terms were treated using an upwind methodology with the weighted integral. The pressure equation was derived from the discrete continuity equation while studying the density-pressure coupling for compressible flow using the pressure-implicit splitting of operators (PISO) as a pressure-velocity coupling technique. The transient terms are discretized for transient analyses using an implicit or backward difference approach. With it, a time step of 100 microseconds was chosen with an iterative time-advancement scheme.

3 GRAIL ENGINE STATIC SIMULATION STUDY

Various tube shape for the intake runners from the reed valve to the inlet valve below the piston is investigated. A 10-psig and 0-psig static pressure boundary were applied to the inlet and outflow respectively. A no-slip requirement was applied to the wall boundary.

On the YZ and XZ planes, Figure 2 displays the velocity vector contour map for all variations of tube configurations. In this illustration, vortices around the intake valve are visible, suggesting the production of tumble vortices on both sides of the intake valve. Several minor vortices can also be seen in the cylinder's XZ plane for all tube configurations.

Journal of Applied Engineering Science

Vol. 20, No. 4, 2022
www.engineeringscience.rs

iipp
publishing

Shoeb Ahmed Syed et al. - Simulation of turbulent flow in a two-stroke grail engine cylinder

The pressure contour map for all three tube configurations is shown in Figure 3. This diagram shows the variation of pressure from the intake channels to tube channels underneath the piston head for various tube configurations. Figures 3 (a) and (b) show that the pressure drops for single- and dual-tube arrangements are around 4–5 psig, respectively, from the original 10 psig. However, as illustrated in Figure 2 (c), the D-tube arrangement results in slight pressure loss. The iso-velocity vectors for all tube configurations are shown in Figure 4.

Conditional to the constraints involved in addressing the sealing of the Grail cycle intake tower, each arrangement has advantages and disadvantages. The D-tube tower configuration accounts for the highest-pressure loss efficiency as well as having the highest mass flow rate of air. Its downside however is the fact that it is the toughest to seal due to its shape.
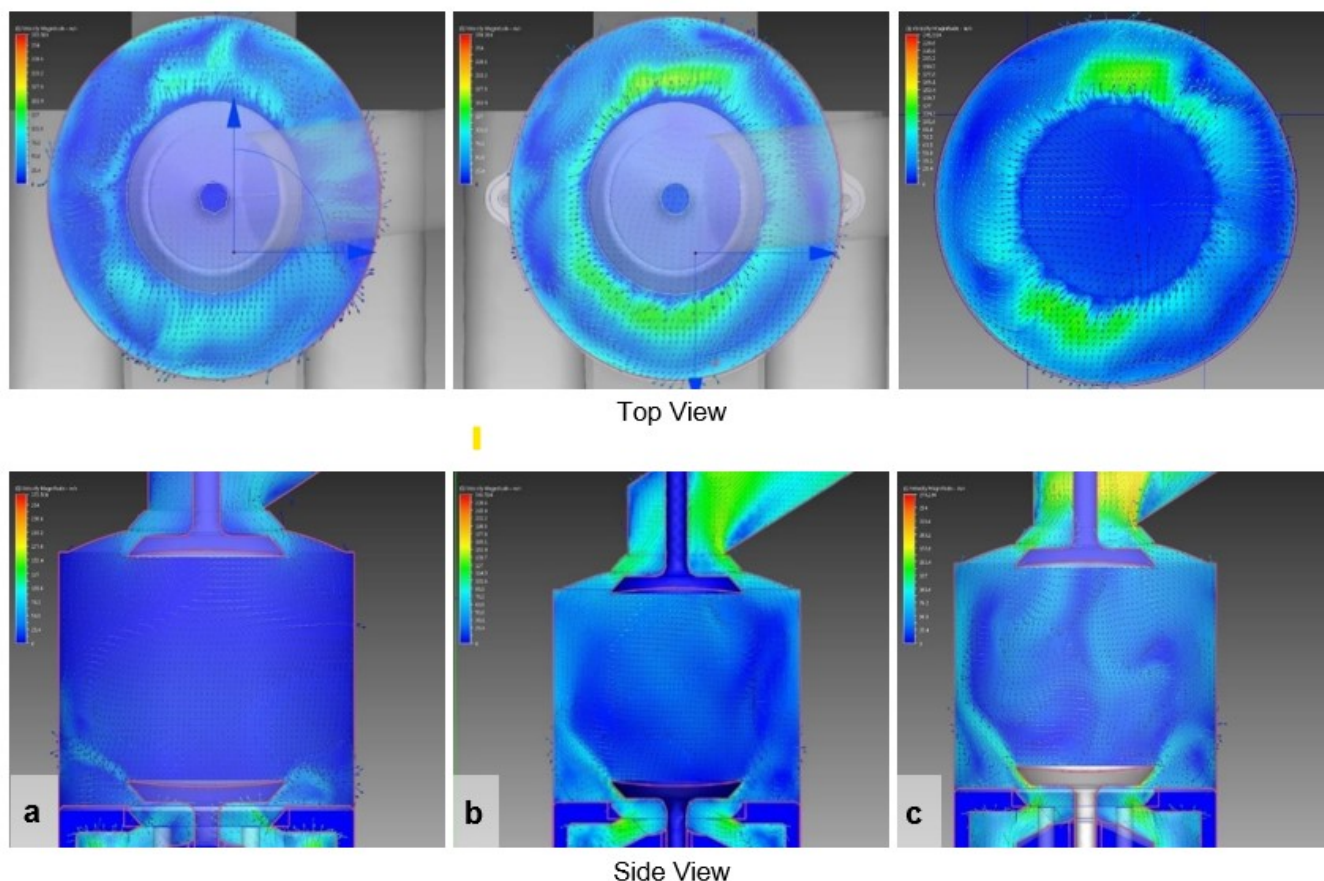

Fig. 2. Velocity vector contour-plots at YZ and XZ planes (a) One-tube (b) Dual-tube (c) D-tube configuration

4 GRAIL ENGINE DYNAMIC SIMULATION STUDY

Figure 3 shows the engine model where the piston head housed the intake valve at its center as well as an exhaust valve centered at the cylinder head. The piston crown is used to investigate the performance, flow pattern, and intensity of turbulence fields within the combustion chamber. The piston shape is based on the genuine Grail engine geometry model, which is used to achieve a better compression ratio and the best combustion process in a Grail engine.

The internal combustion engine's turbulence increases as the RPM rises [4]. As a result, the current CFD simulation is run at a low engine speed of 500 RPM even though the maximum RPM of the engine is restricted to roughly 2000. The CFD calculation's computational domain includes the intake valve and port, exhaust valve and port, piston, and cylinder head as shown in Figure 3.

Near the valve seat, higher mesh densities were formed. Three steps were involved in creating the mesh grid. The computational domain was partitioned into discrete logical pieces in the first stage. Due to the intricacies of geometry, each block was meticulously analyzed. Because physical characteristics such as velocities, pressure, and turbulence intensities change dramatically in the valve seat region, extra attention was required to ensure that the calculations were accurate.

Journal of Applied Engineering Science

Vol. 20, No. 4, 2022

www.engineeringscience.rs

iipp
publishing

Shoeb Ahmed Syed et al. - Simulation of turbulent flow in a two-stroke grail engine cylinder
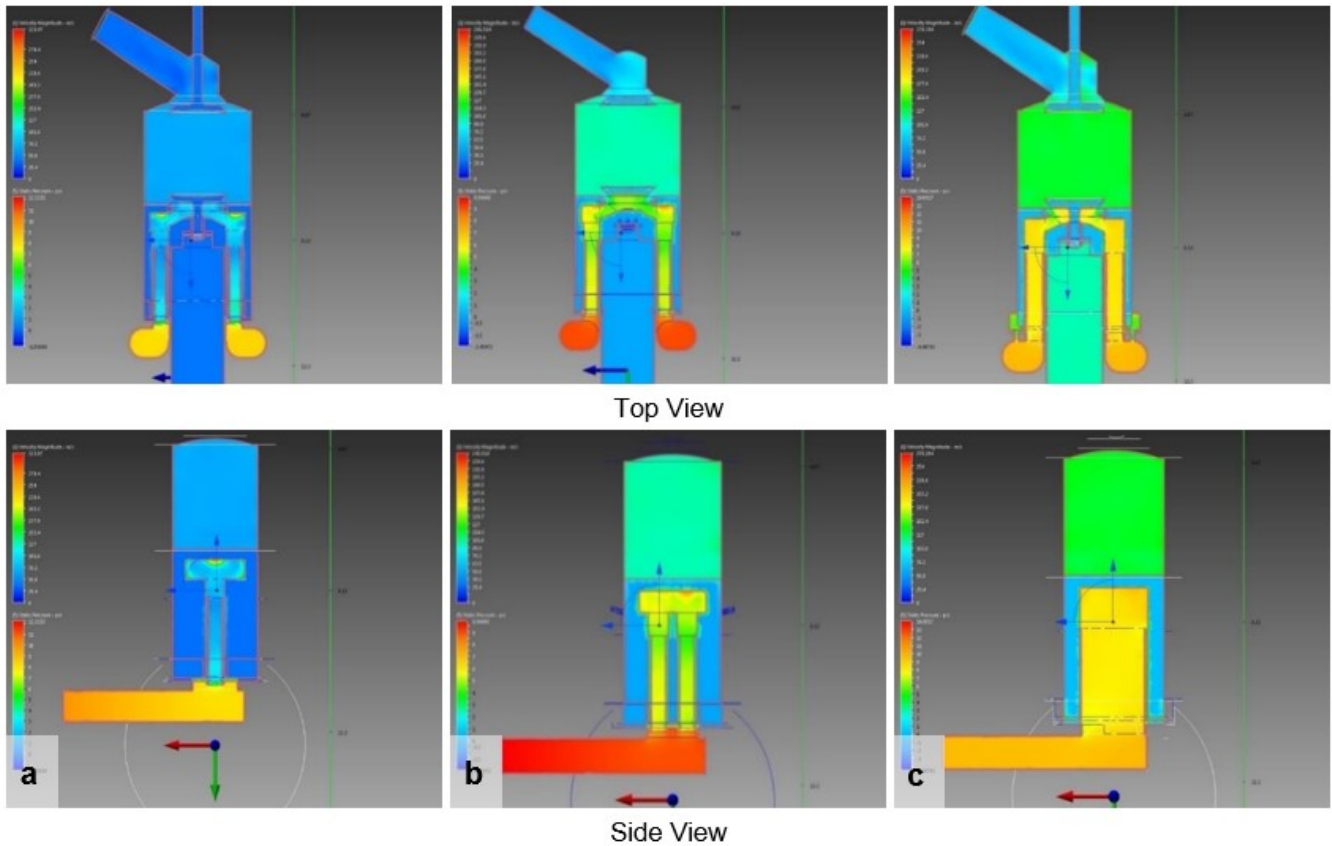
Top View

Side View

Fig. 3. Pressure contour plots at YZ and XZ planes (a) One-tube (b) Dual-tube (c) D-tube configuration

The second sequence involved the formation of the computational grid for all block faces. The final stage was to generate a full mesh of the 3-D volume. Due to the intricacies of engine design and the unstructured mesh requirement, the mesh creation procedure was highly intensive and time-consuming. A 5 million element tetrahedral mesh was created. Given the grid sensitivity and appropriate computer run time, half of the cells were employed to build the mesh at the cylinder head and piston. Moving mesh during valve and piston motion necessitated the fine grid structure.

The inlet valve and the exhaust valve were both in an open position at the start of the simulation. At full open, the inlet and exhaust valves were opened to 0.25 inches. Both the input and exhaust valves, which open from 0 to 0.25 inches, were given a linear motion boundary. Figure 4 depicts the inlet and exhaust valve timings employed in this simulation. A linear sinusoidal motion was applied to the piston at a velocity of 500 RPM. Given that the intake valve was positioned within the piston, its motion was intertwined with that of the piston. To correlate this motion, a simple program was developed.

Fluid flow between the inlet and output boundaries was made possible due to the pressure difference. The intake runners had a 10-psig inlet total pressure while the exhaust tube had a 0 psig exit static pressure (atmospheric).
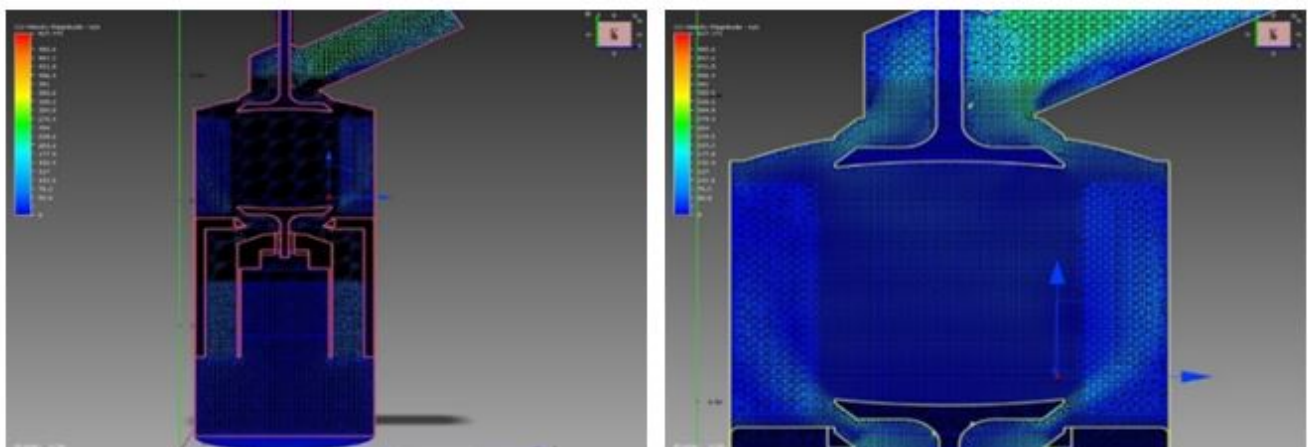

Fig. 4. 2-D Plane Slices Model Mesh

4.1 Simulation Results

The engine compression pressure is shown in figure 5 below. It can be seen that the peak pressure obtained numerically aligns closely with the experimental results which indicate that the CFD analysis, as well as the mesh generations in this study, are an adequate representation for subsequent investigations and turbulence analysis. Additionally, the CFD simulation of the cylinder compression pressure is seen to vary slightly. This is caused by the valve timing difference when it is compared with the values obtained from the experimental setup which is valid for the confirmation of the simulated outcome.
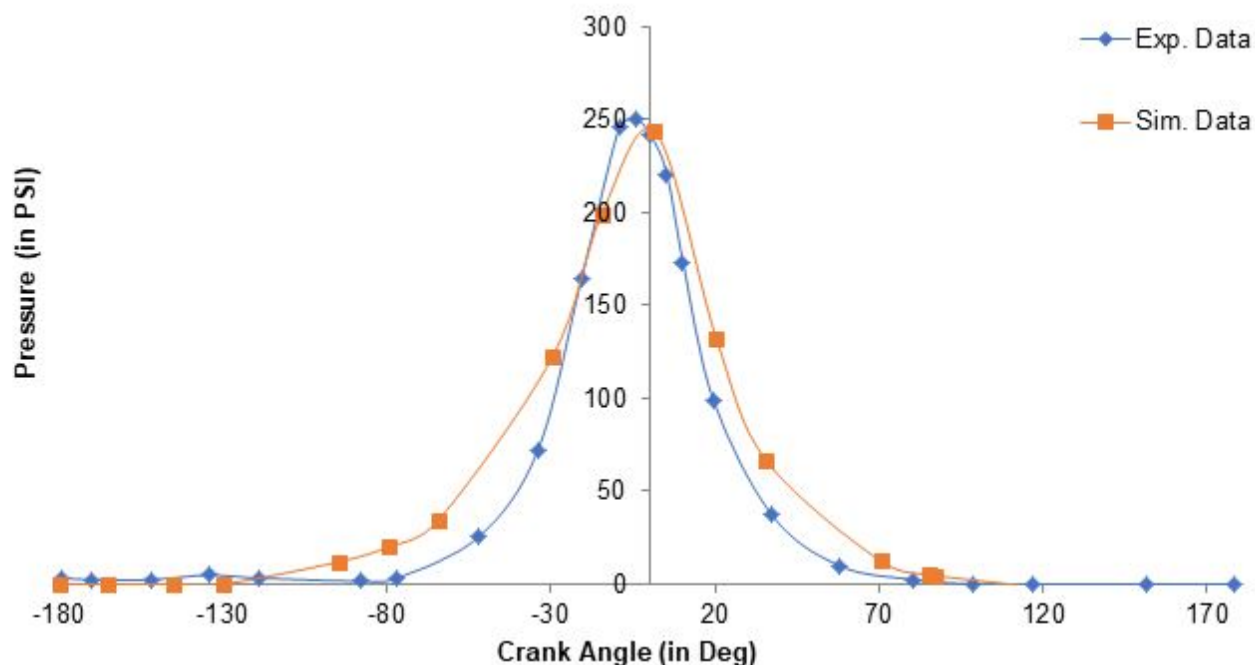

Fig. 5. Compression Pressure Plot for Cylinder Model (Cold Testing)

The flow pattern inside the cylinder for the duration of the compression cycle is shown in figure 6 (d-h) over the central plane at 950 to 00 BTDC. The two vortices which developed toward the end of the suction engine stroke described in the preceding paragraph at 950 BTDC now begin to strike them while forming a bifurcation region in the central region of the cylinder. This region formed may also be a result of the piston's upward movement during the compression stroke which compressed the fluid while reducing the volume in the compression region or combustion chamber up to 300 BTDC. This compression then eliminates the initially created vortices. Figure 6 (g) shows the upward movement of air together with the created vortices while figure 6 (h) indicated the pattern of flow at TDC. This pattern shows the presence of a squish region within the combustion chamber tends to channel the airflow toward the center of the combustion chamber. This generation of vertices combined with the airflow inside the combustion chamber allows for the proper flame spread which ensures effective combustion.

The TKE (m2/s2) which was generated at the intake and compression stroke of the engine was further quantified for the piston which is shown in figure 6 portrays a similar mechanism which is shown in figure 3 above whereas the piston moves towards TDC for compression stroke, the generation of TKE initializes due to the vortices and tumble which releases turbulence energy in the process.

The exponential decrease in the TKE observed in figure 7 during the compression stroke of the Grail engine further indicates that the tumble or vortex stretch phenomenon is not prominent, which is consistent with standard SI engine predictions. For this reason, there is a need for further modification of the Grail engine piston and cylinder head design such that there is an increased tumble effect within the cylinder at TDC. On the other hand, the obtained values of the TKE at TDC from the simulated results show clear similarity within the range of the literature.
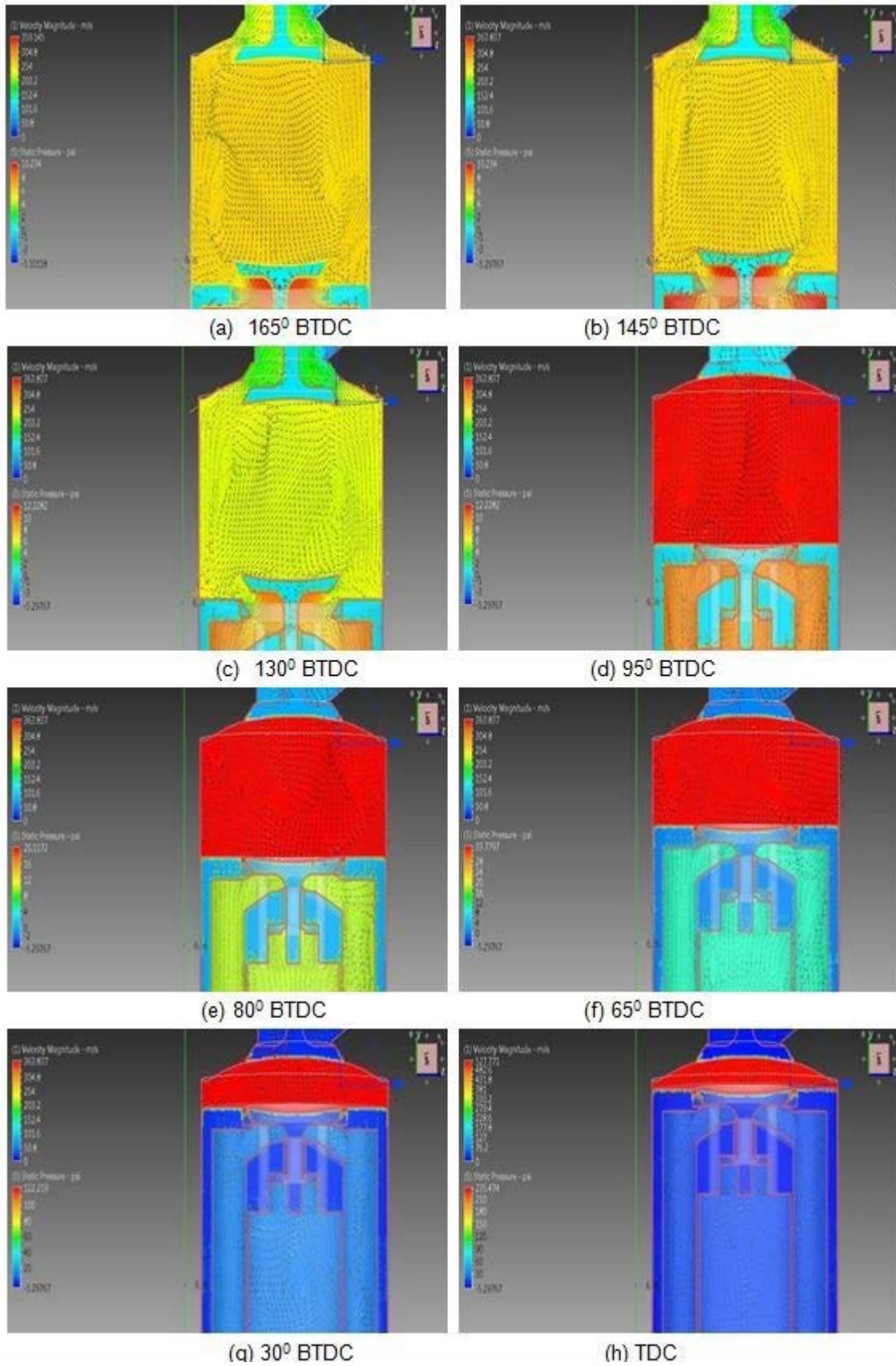
iipp

publishing

Fig.6. Pressure Contour Vector Plotted at Various Crank Angles
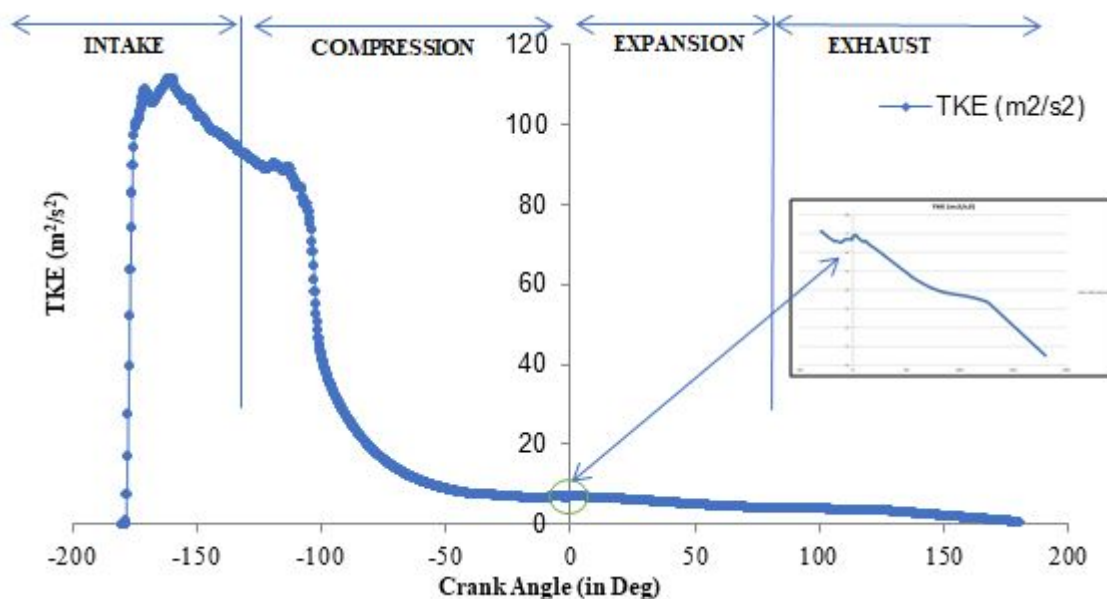
Fig. 7. Engine TKE Plot

From the analysis of turbulence characteristics of the fluid flow at the intake and compression stroke of the engine based on factors such as pressure, axial velocities as well as the degree of crank angles, the intake cycle at 1650 BTDC characterize an increasing pressure due to compression from 950 to 300 BTDC as the exhaust valve outlet closes at 1150 BTDC as seen in figure 6 above. This increased pressure is also experienced at TDC. Figure 6 (a-c) also portrays the velocity vector profiles at an engine speed of 500 RPM. It can be seen that at an intake of 1650 BTDC, the intake valve at the piston top is opened. and the air entering the combustion chamber forms a jet of fluid stream which is virtually parallel to the cylinder head. This fluid jet then bounces off the cylinder side walls which then creates a low-pressure region at the central points of the inlet valve and cylinder giving the predominant airflow around the cylinder walls. This phenomenon results in the generation of two vortex structures that moves in an opposing direction within the cylinder due to the rush and mixing of air rapidly from the high-pressure region along the cylinder walls to the low-pressure zone located at the central part of the cylinder volume. Similarly, this results in the generation of turbulence. The two vortex structures or turbulence flow which are perpendicular to the axis of the cylinder remain in motion while the engine shifts to a compression cycle.

The turbulent Kinetic Energy (TKE) parameter which represents the intake cycle of the engine at 1650 BTDC as well as the compression stroke at TDC when the engine speed is 500 RPM is shown in figure 8. The intake valve on the top of the piston head opens up 1650 to 1150 BTDC from which air enters the combustion chamber from both valve sides. The first three figures a-c show that the maximum or peaked TKE may be caused by the high velocity of the air entering the cylinder which subsequently leads to the jet effect. This value varies almost concerning the mean varying velocities of the airflow. However, the value of the TKE is observed to increase from the cylinder center toward the walls of the chamber given that the airflow from the inlet valves is principally towards the cylinder walls.

The TKE of the engine during the compression stroke is further elaborated in figure 8 (d-h) highlighting the central plane from 950 to 300 BDTC to TDC. The figure shows a uniformly distributed TKE within the cylinder which gradually reduces during compression stroke indicating the disappearance of the tumble. Conclusively, from the results obtained from the CFD analysis investigating the effect of the Grain piston crown, dynamics flow to the turbulence of the engine, this is a sufficient comparison that can be recognized as a genuine CFD result.

Journal of Applied Engineering Science

Vol. 20, No. 4, 2022

www.engineeringscience.rs

iipp
publishing

Shoeb Ahmed Syed et al. - Simulation of turbulent flow in a two-stroke grail engine cylinder

(a) 165⁰ BTDC

(b) 145⁰ BTDC

(c) 130⁰ BTDC

(d) 95⁰ BTDC
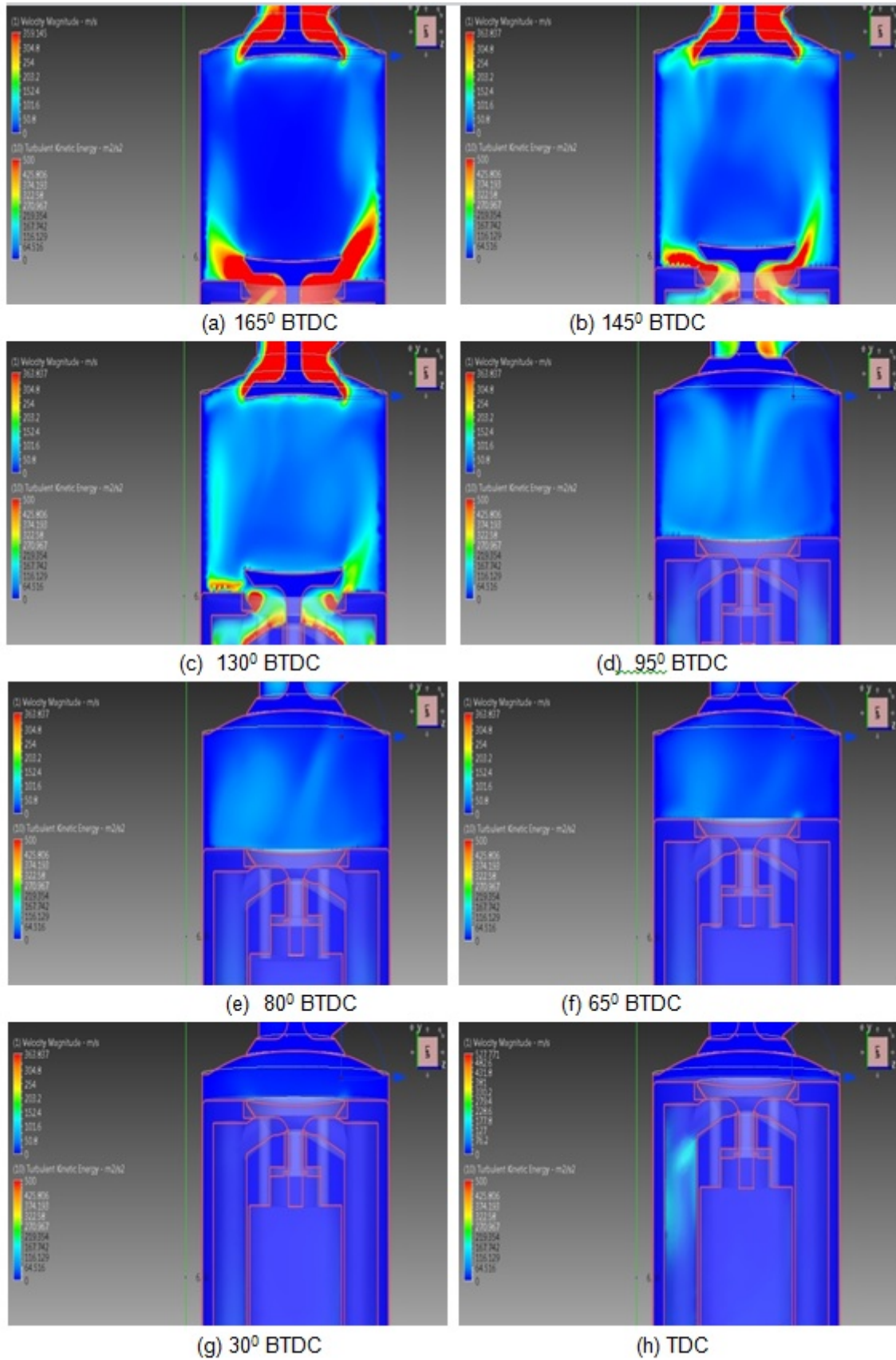
(e) 80⁰ BTDC

(f) 65⁰ BTDC

(g) 30⁰ BTDC

(h) TDC

Fig. 6. TKE Contour Vector Plotted at Various Crank Angles

5 CONCLUSION

This research compares three distinct flow models based on the flow around a fixed intake valve and a piston-cylinder assembly with a top-mounted fixed open valve to CFD simulation of the flow dynamics of the engine. The result of the simulation aligns with the results obtained from experimental data. The later section of the paper is focused on the static and dynamic analysis of the Grail engine. From the CFD analysis, it was concluded that the optimal design

of the piston will be a rectangular hole as well as a D-tube configuration. Furthermore, the efficiency determination criterion was based on the combination of all characteristics i.e., intake swirl flow, minimum drop in pressure in channel flow as well as an ideal mass flow rate within the cylinder. The relevance of the piston crown shape in determining the needed large-scale fluid motion is demonstrated in the dynamic simulation of the engine's intake stroke. Similar to the static analysis in the intake stroke, the simulation anticipated a familiar jet structure and strength between the valves and the cylinder walls. Also, the consequence of compression on fluid flow is negligible all through the engine compression stroke while velocity and TKE rapidly decrease, implying that the breakdown of previously generated tumble experienced in compression is not dominant, implying a redesign of the engine's piston crown as well as cylinder head.

6 REFERENCES

[1] S. A. Syed, "Numerical simulation of turbulent flow inside the cylinder of a new two-stroke grail engine design," PhD Thesis, Wichita State University, 2015.

[2] "US Patent Application for Two-stroke engine Patent Application (Application #20110036313 issued February 17, 2011) - Justia Patents Search." https://patents.justia.com/patent/20110036313 (accessed May 30, 2022).

[3] R. B. Lechner, "Modelling of the combustion parameters of biogenous fuel gases to predict stable combustion conditions in multifuel systems," PhD Thesis, University of Birmingham, 2020.

[4] A. K. Agarwal, S. Gadekar, and A. P. Singh, "In-cylinder air-flow characteristics of different intake port geometries using tomographic PIV," Physics of Fluids, vol. 29, no. 9, p. 095104, 2017.

[5] B. MuraliKrishna and J. M. Mallikarjuna, "Effect of engine speed on in-cylinder tumble flows in a motored internal combustion engine - An experimental investigation using particle image velocimetry," Journal of Applied Fluid Mechanics, 2011, doi: 10.36884/jafm.4.01.11895.

[6] Y. Li, H. Zhao, Z. Peng, and N. Ladommatos, "Particle image velocimetry measurement of in-cylinder flow in internal combustion engines - Experiment and flow structure analysis," Proceedings of the Institution of Mechanical Engineers, Part D: Journal of Automobile Engineering, 2002, doi: 10.1243/0954407021528913.

[7] K. M. Rahman, N. Kawahara, D. Matsunaga, E. Tomita, Y. Takagi, and Y. Mihara, "Local fuel concentration measurement through spark-induced breakdown spectroscopy in a direct-injection hydrogen spark-ignition engine," International Journal of Hydrogen Energy, vol. 41, no. 32, pp. 14283–14292, 2016.

[8] M. R. Abdulwahab, Y. H. Ali, F. J. Habeeb, A. A. Borhana, A. M. Abdelrhman, and S. M. A. Al-Obaidi, "A review in particle image velocimetry techniques (developments and applications)," Journal of Advanced Research in Fluid Mechanics and Thermal Sciences, vol. 65, no. 2, pp. 213–229, 2020.

[9] 김명수, "Development of a Comprehensive 0D Model for an SI Engine Based on the Analysis of the Kinetic Energy of Tumble and the Critical Factors for Flame Wrinkling," PhD Thesis, 서울대학교 대학원, 2022.

[10] J. T. Ilić, S. S. Ristić, and M. Ž. Srećković, "Laser doppler velocimetry and confined flows," Thermal Science, vol. 21, no. suppl. 3, pp. 825–836, 2017.

[11] A. O. Ojo, B. Fond, C. Abram, B. G. Van Wachem, A. L. Heyes, and F. Beyrau, "Thermographic laser Doppler velocimetry using the phase-shifted luminescence of BAM: Eu 2+ phosphor particles for thermometry," Optics express, vol. 25, no. 10, pp. 11833–11843, 2017.

[12] F. Payri, J. Benajes, X. Margot, and A. Gil, "CFD modeling of the in-cylinder flow in direct-injection Diesel engines," Computers and Fluids, 2004, doi: 10.1016/j.compfluid.2003.09.003.

[13] J. B.Heywood, Internal Combustion Engine Fundamentals Second Edition. 2015.

[14] K. Kuwahara and H. Ando, "Diagnostics of in-cylinder flow, mixing and combustion in gasoline engines," Measurement Science and Technology. 2000. doi: 10.1088/0957-0233/11/6/202.

[15] A. A. Verbeek, T. W. Bouten, G. G. Stoffels, B. J. Geurts, and T. H. van der Meer, "Fractal turbulence enhancing low-swirl combustion," Combustion and Flame, vol. 162, no. 1, pp. 129–143, 2015.

[16] K. Pan and J. Wallace, "Soot and combustion models for direct-injection natural gas engines," International Journal of Engine Research, vol. 23, no. 1, pp. 150–166, 2022.

[17] R. K. Maurya and P. Mishra, "Parametric investigation on combustion and emissions characteristics of a dual fuel (natural gas port injection and diesel pilot injection) engine using 0-D SRM and 3D CFD approach," Fuel, vol. 210, pp. 900–913, 2017.

[18] F. J. Laimböck, G. Meister, and S. Grilc, "CFD application in compact engine development," 1998. doi: 10.4271/982016.

[19] H. Hori, T. Ogawa, and T. Kuriyama, "CFD in-cylinder flow simulation of an engine and flow visualization," 1995. doi: 10.4271/950288.

[20] P. Ramaswamy, V. Shankar, V. R. Reghu, N. Mathew, and S. M. Kumar, "A model to predict the influence of inconsistencies in thermal barrier coating (TBC) thicknesses in pistons of IC engines," Materials Today: Proceedings, vol. 5, no. 5, pp. 12623–12631, 2018.

[21] A. Siddique, S. A. Azeez, and R. Mohammed, "Simulation And CFD Analysis of Various Combustion Chamber Geometry of A CI Engine Using CFX," Simulation, vol. 5, no. 8, pp. 33–39, 2016.

[22] S. J. Kazmouz, Large-Eddy Simulations of Motored Flow and Combustion in a Stratified-Charge Direct-Injection Spark-Ignition Engine. The Pennsylvania State University, 2020.

[23] "Discretization Method | CFD | Autodesk Knowledge Network." https://knowledge.autodesk.com/support/cfd/learn-explore/caas/CloudHelp/cloudhelp/2014/ENU/SimCFD/files/GUID-DEE0664D-771B-4446-9ED4-1498267D13FB-htm.html (accessed Apr. 25, 2021).

[24] "General Fluid Flow and Heat Transfer Equations | CFD | Autodesk Knowledge Network." https://knowledge.autodesk.com/support/cfd/learn-explore/caas/CloudHelp/cloudhelp/2014/ENU/SimCFD/files/GUID-83A92AE5-0E9E-4E2D-B61F-64B3696E5F66-htm.html (accessed Apr. 25, 2021).

[25] B. E. LAUNDER and D. B. SPALDING, "THE NUMERICAL COMPUTATION OF TURBULENT FLOWS," in Numerical Prediction of Flow, Heat Transfer, Turbulence and Combustion, 1983. doi: 10.1016/b978-0-08-030937-8.50016-7.